Processing and Application of Ceramics 15 [1] (2021) 11–18
https://doi.org/10.2298/PAC2101011S

Effects of oxidation of SiC aggregates on the sintering behaviour and microstructures of SiC-$CaAl_{12}O_{19}$ composite refractories

Yaochen Si[1], Miao Xia[1], Hongxia Li[1,*], Honggang Sun[1,2,*], Ang Guo[1], Yihao Du[1], Shixian Zhao[1], Xinlian Shang[1], Yongqiang Chen[3,*]

[1]*State Key Laboratory of Advanced Refractories, Sinosteel Luoyang Institute of Refractories Research Co., Ltd., Luoyang 471039 Henan, China*
[2]*School of Materials Science and Engineering, University of Science & Technology Beijing, Beijing 100083, China*
[3]*School of Materials Science and Engineering, Zhengzhou University, Henan, 450001, China*

Received 23 July 2020; Received in revised form 20 November 2020; Accepted 14 December 2020

Abstract

In order to develop chrome-free refractory materials applicable in coal slurry gasification, SiC-$CaAl_{12}O_{19}$ (SiC-CA_6) composite refractories were developed and prepared by using SiC aggregates and CA_6 powders as main raw materials. The sintering behaviour of the composites was investigated. After firing at different temperatures under CO atmosphere, the effects of oxidation of SiC aggregates on the sintering behaviour and microstructures of SiC-CA_6 composite refractories were investigated. SiC-CA_6 composites could not be sintered when firing temperature was lower than 1500 °C. SiC had a passive oxidation and the oxidation components were able to react with CA_6 to form $CaAl_2Si_2O_8$. The $CaAl_2Si_2O_8$ melted into liquid when sintering temperature was in the range of 1500–1600 °C, which promoted the sintering process of the SiC-CA_6 composites. At temperatures above 1600 °C, an active oxidation of SiC occurred. Simultaneously, SiC could also reacted with the $SiO_{2(s,l)}$ to form SiO, leading to the precipitation of Al_2O_3 and CaO in the liquid to generate plate-like CA_6. Above this temperature, the sintering of the SiC-CA_6 composite refractories was affected by the growth of CA_6 and oxidation of SiC. This work demonstrates that the optimal sintering temperature for the SiC-CA_6 composite refractories was 1600 °C.

Keywords: *firing temperature, SiC-CA_6 composite refractories, oxidation, microstructures*

I. Introduction

Coal gasification is an important efficient approach to the clean utilization of coal [1]. At present, the coal gasifiers work between 1300 and 1600 °C at pressures of 2–9 MPa under a strongly reducing atmosphere [2–5]. During the coal gasification process, the refractory lining of gasifiers will be attacked by the molten coal slag. Therefore, the refractories used in the gasifiers not only require excellent coal slag penetration and corrosion resistance, but also need excellent mechanical strength to bear the enormous thermal stress and abrasion [6,7]. Because of harsh working conditions in the coal gasifiers, the refractories used in gasifiers usually have an open porosity between 15 and 18%. Also, the bending strength (CMOR) should be about 10 MPa or higher to withstand the high pressure and the self-weight of the lining [8,9]. In general, chrome-containing refractories are used as lining materials due to their great high temperature strength, excellent slag penetration and corrosion resistance. However, Cr_2O_3 may react with CaO, Na_2O or K_2O to form Cr^{6+} [1], which has adverse effects on the environmental protection and human health. Thus, environment-friendly low-chromium or chrome-free refractories for coal gasifiers have become a major subject for sustainable development of coal chemical industries.

SiC has high melting point, good thermal stability,

* Corresponding author: tel: +86 13503497128,
e-mail: *lihongx0622@126.com* (Hongxia Li)
sunhonggang@hotmail.com (Honggang Sun)
15294628626@163.com (Yongqiang Chen)

excellent erosion resistance, slag resistance and other characteristics [10–12], revealing an important application prospect in coal gasifiers. However, sintering of SiC-containing materials is difficult due to the strong covalent nature of Si–C bond and the oxidation of SiC [13–15]. Calcium hexaluminate ($CaAl_{12}O_9$, abbreviated as CA_6) has plate-like structure, excellent high temperature mechanical properties, strong stability in reducing atmosphere at high temperature, and especially good chemical stability in alkaline environment [16–18]. Therefore, CA_6 has been applied in steel making, petrochemical and other fields as a new synthetic raw material in recent years. Considering the operating environment of coal gasification, the development of SiC and CA_6 composite materials as refractory lining of gasifier is supposed to be an alternative to chromium-containing refractories for coal gasification.

When SiC aggregates coexist with oxide matrix, the sintering process of the composites is complex [19]. Since SiC might oxidise to SiO_2, and if there were Al_2O_3 and CaO in the materials, SiO_2 could react further with them to form low melting point phase [20], which could promote the sintering of the materials at a high temperature. In this paper, SiC-CA_6 composite refractories were prepared by using fused SiC particles as aggregates and sintered CA_6 powders as matrix. The as-prepared composite refractories were fired in the temperature range of 1300–1650 °C under CO atmosphere. The effects of oxidation of SiC aggregates on the sintering behaviour and microstructures of the SiC-CA_6 composite refractories were investigated.

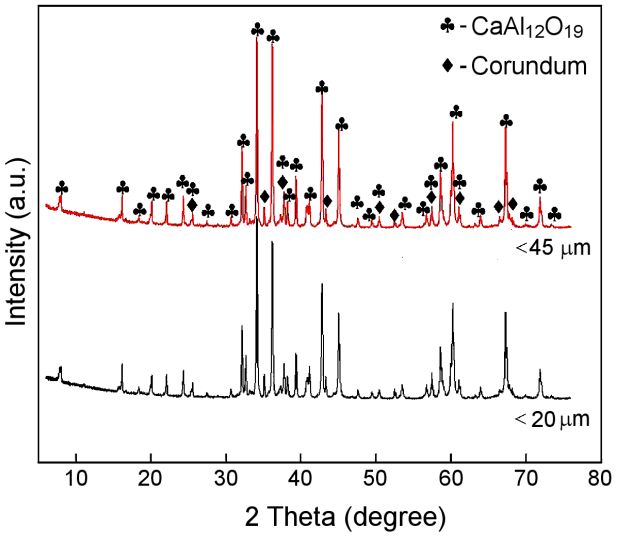

Figure 1. XRD patterns of CA_6 raw materials

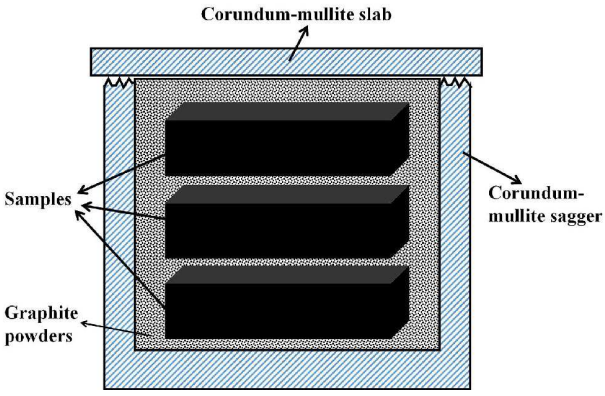

Figure 2. Carbon-rich conditions

II. Experimental

2.1. Raw materials

Commercial SiC (98 wt.%, Luoyang Naiyan Industry and Trade Co., Ltd, China) powders (with particle sizes of 2.5–1.43 mm, 1.43–0.5 mm, ≤ 0.5 mm) and sintered CA_6 powders with sizes of 45 μm and 20 μm were used as main raw materials. XRD patterns of the CA_6 raw materials (Fig. 1) show that the main phases were CA_6 and corundum. The chemical compositions of these raw materials are shown in Table 1.

2.2. Sample preparation

According to the formulation of the specimens listed in Table 2, these raw materials were accurately weighed and mixed with an organic resin as binder. After 24 h ageing, the mixtures were pressed to prismatic samples with dimensions of 25 × 25 × 150 mm with the pressure of 100 MPa. Then, all prepared samples were dried at 110 °C for 12 h and completely embedded into the graphite bed powder in a corundum-mullite crucible (Fig. 2). Finally, all the samples were fired at 1300, 1400, 1500, 1550, 1600 and 1650 °C for 3 h.

2.3. Characterization

The weight change of the samples was calculated using Eq. 1 below:

Table 1. The chemical components of the raw materials

Raw material	Chemical composition [wt.%]										
	SiC	C	Si	Fe_2O_3	Al_2O_3	MgO	CaO	SiO_2	Na_2O	TiO_2	K_2O
SiC	98.51	0.36	0.22	0.30	-	-	-	-	-	-	-
CA_6	-	-	-	0.06	88.94	0.92	7.98	0.86	0.28	0.04	0.01

Table 2. Formulations of specimens

Raw materials	SiC			CA_6		Organic resin
	2.5–1.43 mm	1.43–0.5 mm	≤0.5 mm	45 μm	20 μm	
Content [wt.%]	30	20	15	20	15	+4

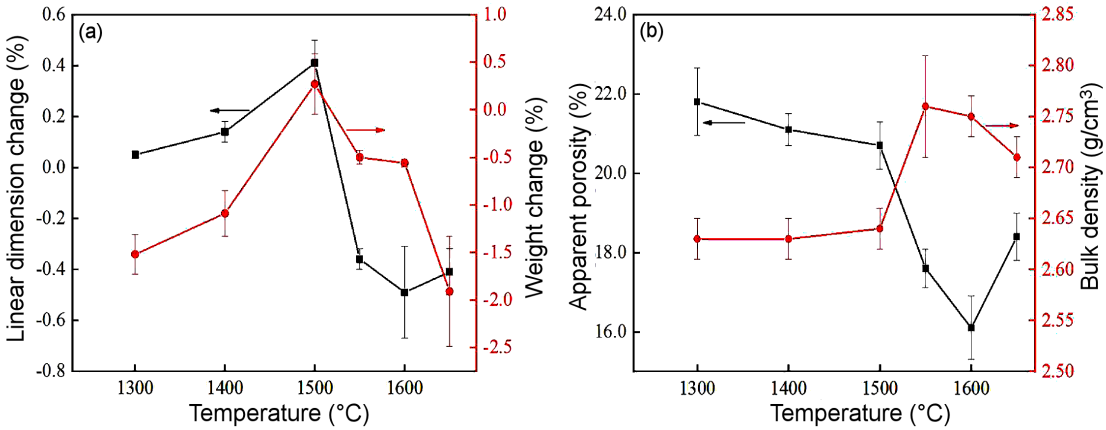

Figure 3. Sintering behaviour of samples after firing at different temperatures: a) linear dimension change and the mass change and b) apparent porosity and bulk density

$$W_C = \frac{W_1 - W_0}{W_0} \cdot 100 \qquad (1)$$

where W_C represents the weight change of the samples, W_0 and W_1 are the weight of the samples before and after the heat treatment, respectively.

The linear dimension change of all the samples was measured according to the Chinese Standard GB/T 5988-2007. The apparent porosity and bulk density of the samples were measured by the Archimedes' method in accordance with the Chinese Standard GB/T 2997-2015. The phase composition of the fired samples was investigated by X-ray diffraction (XRD, Empyrean, PAN Analytical Company). The microstructures and chemical components of the samples were examined by SEM (EVO-18, Zeiss Company) and EDS (X-Max50, Oxford Company). The mercury intrusion instrument (AutoPore IV 9500, American Micrometrics Instrument Corporation) with the filling pressure from 0.1 to 60000 psi was used to measure the pore size distributions of the samples fired at different temperatures.

III. Results and discussion

3.1. Sintering behaviour

Figure 3 shows the sintering behaviour of the samples fired for 3 h at different temperatures. As it could be seen from Fig. 3a, the linear dimension change and the weight change of the samples increase at first and then decrease with the increase of firing temperature. It seems that 1500 °C is the turning point for the sintering behaviour of these samples in the experiments. Below 1500 °C, the samples showed expansion and gained some weight, the apparent porosity and bulk density of the samples had changed a little (Fig. 3b). When the firing temperatures exceeded 1500 °C, the samples showed shrinkage and weight loss. The shrinkage of the samples reached the maximum value at 1600 °C while

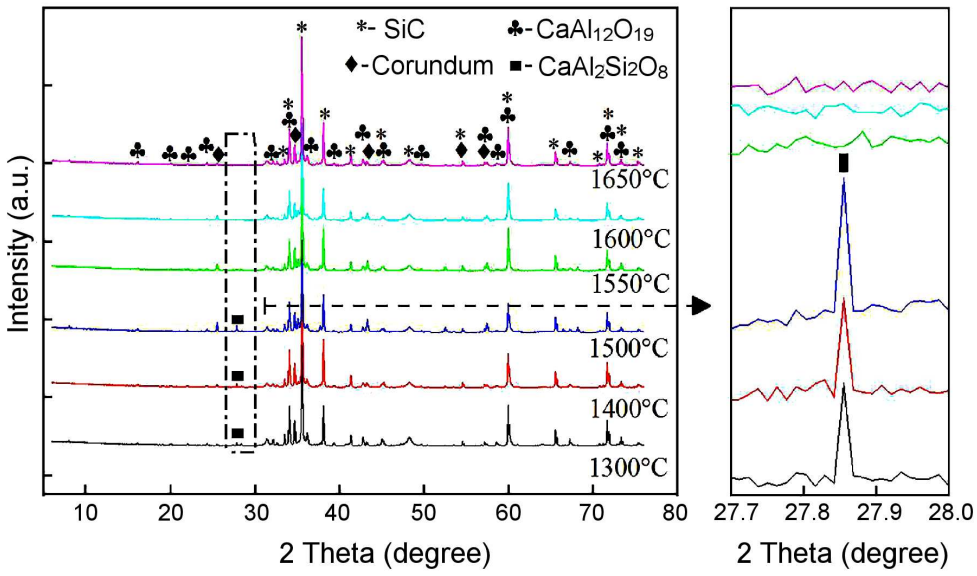

Figure 4. XRD patterns of samples after firing at different temperatures

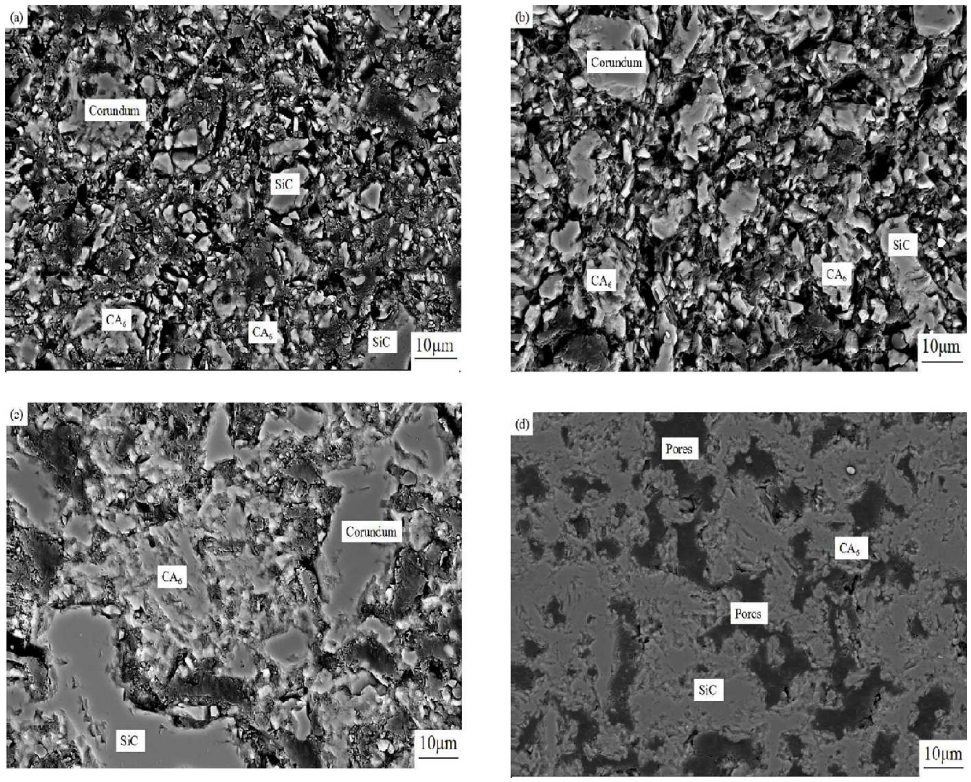

Figure 5. SEM images of the specimens sintered at: a) 1400 °C, b) 1500 °C, c) 1600 °C and d) 1650 °C

weight loss was continuously increased. However, the linear dimension change increased when temperature was higher than 1600 °C. The apparent porosity of the samples had the same tendency with the linear dimension change (Fig. 3b).

3.2. Phase evolution and microstructures

Figure 4 shows XRD patterns of the SiC-CA_6 composite refractories fired at different temperatures. The main phases of the samples fired at different temperatures were SiC, CA_6 and a small amount of corundum. In addition, anorthite ($CaAl_2Si_2O_8$) formed showing weak peaks when firing temperature was lower than 1550 °C.

The microstructures of the samples fired in the temperature range of 1400 to 1650 °C are shown in Fig. 5. It could be seen that the interface between SiC particles and CA_6 fine powders was very clear after firing at 1400 and 1500 °C (Fig. 5a and 5b). In addition, the edges of fine CA_6 powders in the matrix were also distinctive with a little amount of CA_6 sintered together. As the firing temperature was raised continuously up to 1600 °C (Fig. 5c), tiny granular crystals in the matrix bonded not only with each other but also with the surrounding particles in large quantities, resulting in a large number of bonded granular crystals. However, when the samples were fired at 1650 °C (Fig. 5d), besides the sintered matrix, it could be also seen that much more large pores formed partially connected when compared with the samples fired at 1600 °C.

By comparing Fig. 5d with 5b and 5c, it could be found that the pore size distribution changed obviously with the increase of temperature as shown in Fig. 6. The average pore size was much smaller when fired at 1500 °C. When temperature increased, the pore size increased accordingly, but the amount of total pores was decreased significantly. However, when temperature exceeded 1600 °C, the content of large pores was much higher. The average pore diameters of the samples fired at 1500, 1600 and 1650 °C were 0.6, 1.0 and 6.3 μm, respectively.

In order to further understand the microstructure evolution of the samples, the fracture surfaces of the samples fired at 1500, 1600 and 1650 °C are shown in Fig. 7

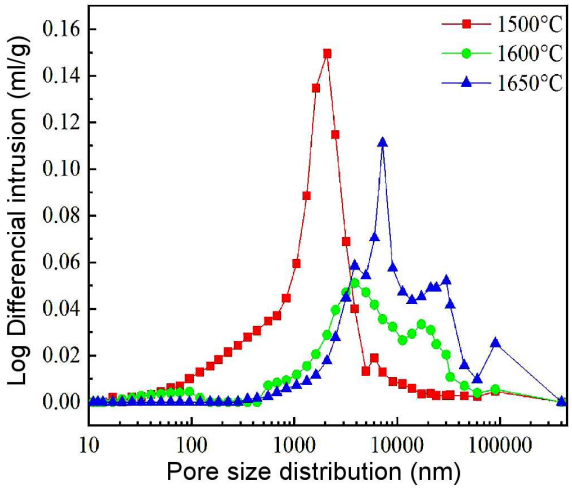

Figure 6. Pore size distributions of the samples sintered at 1500, 1600 and 1650 °C

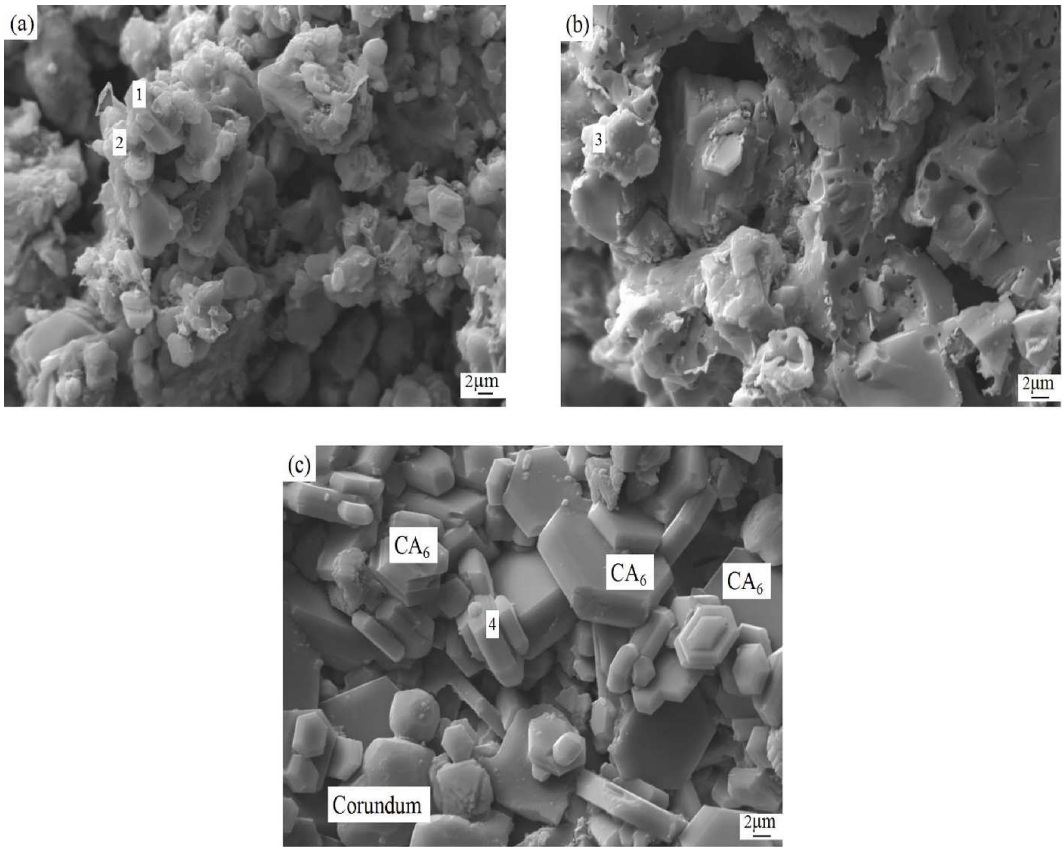

Figure 7. Fracture surfaces of the samples sintered at: a) 1500 °C, b) 1600 °C and c) 1650 °C

Table 3. Chemical compositions of the points in Fig. 7

Location	Content [wt.%]			
	Al_2O_3	SiO_2	CaO	Total
1	87.76	5.05	7.19	100.00
2	70.38	16.60	13.03	100.00
3	60.94	23.95	15.10	100.00
4	87.66	4.23	8.11	100.00

and the EDS analyses of the points in Fig. 7 were shown in Table 3. It can be seen that the samples had low density and inhomogeneous microstructure at 1500 °C. Most of CA_6 grains had granular morphologies and few of them had the plate-like structure (point 1). The floccules (point 2) appearing in the microstructure shown in Fig. 7a were examined by EDS which indicated that grassy phase mainly composed of Al, Si, Ca and O elements. When firing temperature increased to 1600 °C (Fig. 7b), the samples became denser and the grains combined together, which might be due to the formation of liquid at this temperature and the liquid promoted the sintering of the samples. Additionally, it could also be found from the EDS analysis that the SiO_2 content increased in the grassy phase (point 3). However, it could be clearly seen that the grassy phase disappeared and plate-like structure of CA_6 grains formed in the matrix when temperature increased to 1650 °C (Fig. 7c). From the EDS analysis of point 4 in Fig. 7c, it could be found that small amount of SiO_2 along side the CA_6 grains still exists.

IV. Discussion

In this study, carbon-rich atmosphere should be regarded during the experimental procedure. Since the crucible was not completely sealed, oxygen could get into the crucible during the heating process. Under these conditions, carbon would react with oxygen to form CO, i.e. $C_{(s)} + 0.5\,O_{2(g)} \longrightarrow CO_{(g)}$. Therefore, the experimental environment could be considered as a CO rich atmosphere, and CO gas partial pressure (P_{CO}) is about 0.035 MPa. Oxidizing reactions of SiC in the SiC-CA_6 composites could be described as follows [21,22]:

$$SiC_{(s)} + CO_{(g)} \longrightarrow SiO_{(g)} + 2\,C_{(s)} \quad (2)$$

$$SiO_{(g)} + CO_{(g)} \longrightarrow SiO_{2(s)} + C_{(s)} \quad (3)$$

$$SiC_{(s)} + 2\,CO_{(g)} \longrightarrow SiO_{2(s)} + 3\,C_{(s)} \quad (4)$$

$$\Delta G_4^{\theta} = -603150 + 331.983T\ [J \cdot mol^{-1}] \quad (5)$$

In this experimental environment, when firing temperature was lower than 1500 °C, SiC in local area of the samples underwent passive oxidation, which was carried out through Eqs. 2 and 3, or directly through Eq. 4. This conclusion could also be explained from the mass change shown in Fig. 3a. The $SiO_{2(s)}$ was generated and filled the pores in the samples, preventing the further oxidation of SiC inside the samples. Meanwhile, SiO_2 could further react with CA_6 to form $CaAl_2Si_2O_8$ (Eq. 6), as also shown in Fig. 4. In addition, the amount of $CaAl_2Si_2O_8$ increased simultaneously with the in-

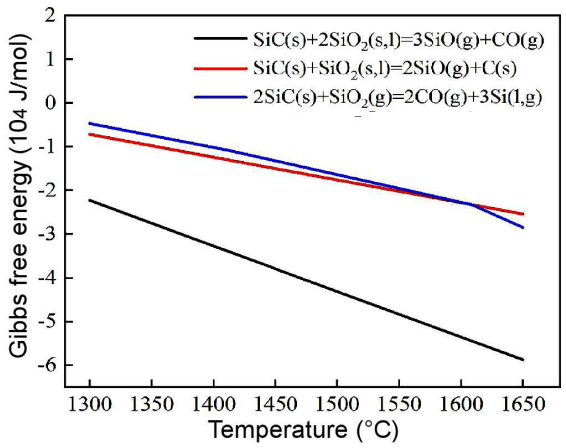

Figure 8. The Gibbs free energy of reactions given in Eqs. 7-9

crease of temperature, resulting in the increase of weight change of samples compared to that at 1300 °C. Although $SiO_{2(s)}$ was formed after firing at 1300–1500 °C, the density of samples changed a little or not at all because the samples had not yet started sintering as seen in Figs. 5a and 5b. When temperature exceeded 1500 °C, the SiC in the samples could undergo an active oxidation through Eq. 2 [22] in some areas while in other areas still having passive oxidation. Besides, the existing $CaAl_2Si_2O_8$ (with a melting point of 1557 °C [23]) could melt to form liquid phase and the samples could began to sinter, causing shrinkage of samples and reducing apparent porosity as well as improving density. This is consistent with the variation of pore size distribution as shown in Fig. 6.

$$2\,SiO_{2(s)} + CaAl_{12}O_{19(s)} \longrightarrow CaAl_2Si_2O_{8(s)} + 5\,Al_2O_{3(s)} \quad (6)$$

However, when firing temperature was above 1600 °C, the active oxidation of SiC happened as the main reaction process through the Eqs. 7-9 [24–28]. The ΔG_r results indicate that all these reactions can occur spontaneously under the test conditions as shown in Fig. 8 and that ΔG_r of Eq. 9 had a turning point as the Si gas formed when temperature is higher than 1600 °C. The synchronously formed $SiO_{(g)}$ and $Si_{(g)}$ might cause the increase of porosity as well as the decrease of density as shown in Fig. 3b, which could also be proved by the variation of the pore size distribution through 1600 to 1650 °C. Furthermore, the SiO_2 in the liquid would also react with the CO (Eq. 10) to form $SiO_{(g)}$ which could escape from the samples [29,30], leaving to the remained $Al_2O_{3(l)}$ and $CaO_{(l)}$ in the liquid. Thereafter, the CA_6 grains with plate-like morphologies could be precipitated from the liquid as shown in Fig. 7c.

$$SiC_{(s)} + 2\,SiO_{2(s,l)} \longrightarrow 3\,SiO_{(g)} + CO_{(g)} \quad (7)$$

$$SiC_{(s)} + SiO_{2(s,l)} \longrightarrow 2\,SiO_{(g)} + C_{(s)} \quad (8)$$

$$2\,SiC_{(s)} + SiO_{2(s,l)} \longrightarrow 2\,CO_{(g)} + 3\,Si_{(l,g)} \quad (9)$$

$$SiO_{2(l)} + CO_{(g)} \longrightarrow SiO_{(g)} + CO_{2(g)} \quad (10)$$

The schematic illustration of microstructures development during the sintering process is shown in Fig. 9. When firing temperature is lower than 1500 °C, SiC undergoes a passive oxidation and the oxidation components can react with CA_6 to form $CaAl_2Si_2O_8$. When sintering temperature is in the range of 1500–1600 °C, $CaAl_2Si_2O_8$ melts into liquid, which promotes the sintering process of SiC-CA_6 composites. At temperatures above 1600 °C, SiC can react with CO in the atmosphere and SiO_2 in the liquid, leading to the formation of plate-like CA_6 from the liquid.

V. Conclusions

According to the published papers [13,14], the passive oxidation production of SiC can generate a protective film to protect the material and the active oxidation production of SiC can cause the constantly con-

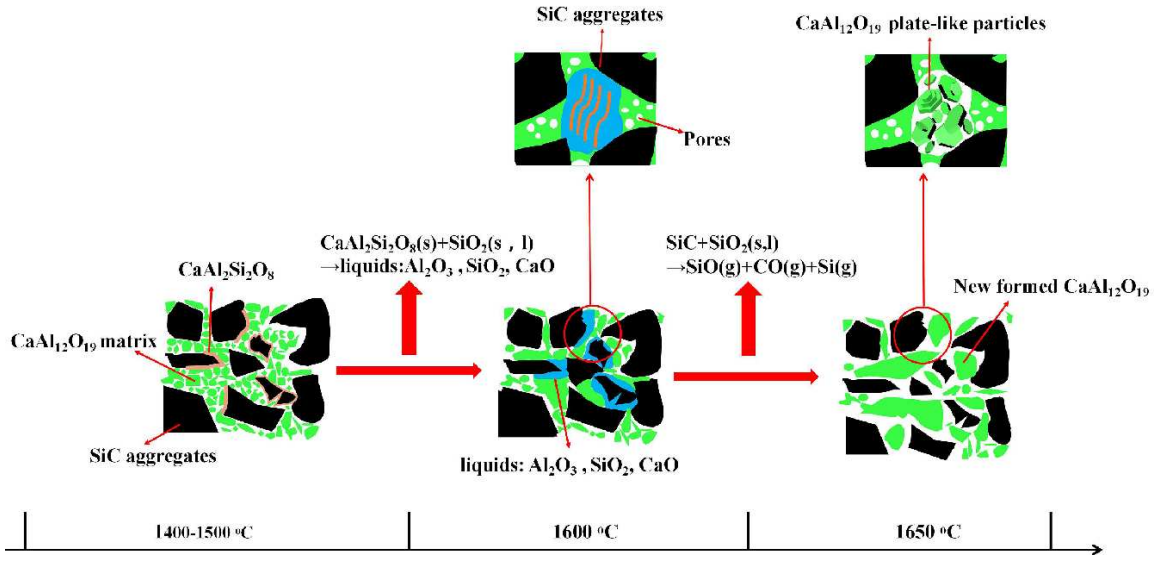

Figure 9. Schematic illustration of microstructures development during the sintering process, representing the difference between 1600 and 1650 °C

sumption of the materials. But in this paper, it could be found that the passive and active oxidation of SiC both had some good effects on the SiC-CA_6 composite refractories. Therefore, the following conclusions were drawn by investigating the effects of oxidation of SiC aggregates on the sintering behaviour and microstructural evolution of the SiC-CA_6 composite refractories after firing at different temperatures under carbon-rich atmosphere.

(1) When firing temperature was lower than 1500 °C, the oxidation of SiC in the SiC-CA_6 composite refractories was controlled in the region of passive oxidation and $CaAl_2Si_2O_8$ was formed via the reaction with generated SiO_2. The SiC-CA_6 composite refractories showed expansion and weight gain, but a little change in their density. Crucially, sintering of the SiC-CA_6 composite refractories did not start under this condition.

(2) In the temperature range of 1500 to 1600 °C, the active oxidation of SiC-CA_6 composite refractories occurred and SiC also had a passive oxidation inside the refractories. The oxidation products SiO_2 and the existing $CaAl_2Si_2O_8$ were incorporated into the liquid as low-melting phases. The liquid promoted the sintering of the SiC-CA_6 composite refractories and caused the shrinkage and increase in the density.

(3) At temperatures above 1600 °C, the active oxidation of the SiC-CA_6 composite refractories occurred as the predominant process and gaseous SiO was generated. SiC in the composite refractories could also react with $SiO_{2(l)}$ to form much more $SiO_{(g)}$, leading to a greater amount of the remaining $Al_2O_{3(l)}$ and $CaO_{(l)}$ in the liquid. Then the CA_6 plate-like particles were precipitated. Under this condition, the oxidation of SiC and growth of CA_6 had a synergistic effect on SiC-CA_6 composite refractories, which caused the expansion of the composites and decrease of density.

Therefore, the results showed that the SiC-CA_6 composite refractories fired at 1600 °C for 3 h under carbon-rich atmosphere had a better sinterability. For the gasifiers applications, the SiC-CA_6 composite refractories will be further studied to improve their properties and corrosion resistance in our future work.

Acknowledgements: This work was financially supported by the Key Program for Henan Joints Funds of the National Natural Science Foundation of China (U1604252).

References

1. B. Cai, H. Li, S. Zhao, H. Sun, P. Li, S. Yan, L. Wan, G. Wan, Z. Cao, "Study on the erosion mechanism of acid coal slag interactions with silicon carbide materials in the simulated atmosphere of a coal gasifier", *Ceram. Int.*, **43** (2017) 4419–4426.
2. J. Nakano, S. Sridhar, J. Bennett, K.-S. Kwong, T. Moss, "Interactions of refractory materials with molten gasifier slags", *Int. J. Hydrogen Energy*, **36** (2011) 4595–4604.
3. B. Cai, H. Li, S. Zhao, H. Sun, G. Wang, Z. Cao, "Thermodynamic calculation of oxygen partial pressure and stability of Cr_2O_3 in coal gasifiers", *Refractories*, **50** (2016) 411–415.
4. B. Cai, H. Li, S. Zhao, H. Sun, P. Li, S. Yan, Y. Du, G. Wang, Z. Cao, "Corrosion of high chromia refractory materials by basic coal slag under simulated coal gasification atmosphere", *Ceram. Int.*, **44** (2018) 4592–4602.
5. K. Kwong, A. Petty, J. Bennett, R. Krabbe, H. Thomas, "Wear mechanisms of chromia refractories in slagging gasifiers", *Int. J. Appl. Ceram. Technol.*, **4** (2007) 503–513.
6. Y. Choi, T. Mun, M. Cho, J. Kim, "Gasification of dried sewage sludge in a newly developed three-stage gasifier: Effect of each reactor temperature on the producer gas composition and impurity removal", *Energy*, **114** (2016) 121–128.
7. R. Williford, K. Johnson, K. Sundaram, "Modelling of high-chromia refractory spalling in slagging coal gasifiers", *Ceram. Int.*, **34** (2008) 2085–2089.
8. M. Müller, K. Hilpert, L. Singheiser, "Corrosion behaviour of chromium-free ceramics for liquid slag removal in pressurized pulverized coal combustion", *J. Eur. Ceram. Soc.*, **29** (2009) 2721–2726.
9. P. Gehre, C. G. Aneziris, "Investigation of slag containing refractory materials for gasification processes", *J. Eur. Ceram. Soc.*, **32** (2012) 4051–4062.
10. H. Wang, Y. Bi, N. Zhou, H. Zhang, "Preparation and strength of SiC refractories with in situ β-SiC whiskers as bonding phase", *Ceram. Int.*, **42** (2016) 727–733.
11. Y. Hirata, H. Shirai, R. Ando, Y. Matsumoto, T. Shimonosono, "Theoretical and experimental analyses of relationship between processing and thermal conductivity of SiC with oxide additives", *Ceram. Int.*, **42** (2016) 13612–13624.
12. N. Song, H. Zhang, H. Liu, J. Fang, "Effects of SiC whiskers on the mechanical properties and microstructure of SiC ceramics by reactive sintering", *Ceram. Int.*, **43** (2017) 6786–6790.
13. N. Jacobson, B. Harder, D. Myers, M. Cinibulk, "Oxidation transitions for SiC Part I. Active-to-passive transitions", *J. Am. Ceram. Soc.*, **96** (2013) 838–844.
14. B. Harder, N. Jacobson, D. Myers, M. Cinibulk, "Oxidation transitions for SiC Part II. Passive-to-active transitions", *J. Am. Ceram. Soc.*, **96** (2013) 606–612.
15. A. Gallet-Doncieux, O. Bahloul, C. Gault, M. Huger, T. Chotard, "Investigations of SiC aggregates oxidation: Influence on SiC castables refractories life time at high temperature", *J. Eur. Ceram. Soc.*, **32** (2012) 737–743.
16. C. Domínguez, R. Torrecillas, "Influence of Fe^{3+} in the sintering and microstructural evolution of reaction sintered calcium hexaluminate", *J. Eur. Ceram. Soc.*, **18** (1998) 1373–1379.
17. X. Liu, D. Yang, Z. Huang, S. Yi, H. Ding, M. Fang, S. Zhang, Y. Liu, "Novel synthesis method and characterization of porous calcium hexa-aluminate ceramics", *J. Am. Ceram. Soc.*, **97** (2014) 2702–2704.
18. R. Salomão, V.L. Ferreira, L.M.M. Costa, I.R. de Oliveira, "Effects of the initial CaO-Al_2O_3 ratio on the microstructure development and mechanical properties of porous calcium hexaluminate", *Ceram. Int.*, **44** (2018) 2626–2631.
19. A. Gallet-Doncieux, O. Bahloul, C. Gault, M. Huger, T. Chotard, "Investigations of SiC aggregates oxidation: influence on SiC castables refractories life time at high temperature", *J. Eur. Ceram. Soc.*, **32** (2012) 737–743.
20. S. Takahashi, D.R. Neuville, H. Takebe, "Thermal properties, density and structure of percalcic and peralumi-

nus CaO-Al_2O_3-SiO_2 glasses", *J. Non-Cryst. Solids*, **411** (2015) 5–12.
21. Z.Y. Chen, "Chemical thermodynamics of refractories", *Metallurgical Industry Press*, Beijing, 2005, 539. (in Chinese).
22. B. Ma, Q. Zhu, Y. Sun, J. Yu, Y. Li, "Synthesis of Al_2O_3-SiC composite and its effect on the properties of low-carbon MgO-C refractories", *J. Mater. Sci. Technol.*, **26** (2010) 715–720.
23. H. Zuo, C. Wang, Y. Liu, "Dissolution behavior of a novel Al_2O_3-SiC-SiO_2-C composite refractory in blast furnace slag", *Ceram. Int.*, **43** (2017) 7080–7087.
24. R. Clarke, "On the equilibrium thickness of intergranular glass phase in ceramics materials", *J. Am. Ceram. Soc.*, **70** (1987) 15–22.
25. N.S. Jacobson, K.N. Lee, D.S. Fox, "Reactions of silicon carbide and silicon (IV) oxide at elevated temperatures", *J. Am. Ceram. Soc.*, **75** (1992) 1603–1611.
26. T. Goto, H. Homma, "High-temperature active/passive oxidation and bubble formation of CVD SiC in O_2 and CO_2 atmospheres", *J. Eur. Ceram. Soc.*, **22** (2002) 2749–2756.
27. G. Honstein, C. Chatillon, F. Baillet, "Thermodynamic approach to the vaporization and growth phenomena of SiC ceramics. I. SiC and SiC-SiO_2 mixtures under netural conditions", *J. Eur. Ceram. Soc.*, **32** (2012) 1117–1135.
28. G. Honstein, C. Chatillon, F. Baillet, "Thermodynamic approach to the vaporization and growth phenomena of SiC ceramics. II. The SiC surface under oxidative conditions", *J. Eur. Ceram. Soc.*, **32** (2012) 1137–1147.
29. M.M. Shul'ts, S.I. Shornikov, V.L. Stolyarova, "Evaporation processes and thermodynamic properties of mullite", *Dokl. Phys. Chem.*, **336** [1-3] (1994) 95–98.
30. Y. Orooji, E. Ghasali, M. Moradi, M.R. Derakhshandeh, M. Alizadeh, M.S. Asl, T. Ebadzadeh, "Preparation of mullite-TiB_2-CNTs hybrid composite through spark plasma sintering", *Ceram. Int.*, **45** (2019) 16288–16296.